Biomedical Optics EXPRESS

Quantitative phase spectroscopy

Matthew Rinehart,* Yizheng Zhu, and Adam Wax

Department of Biomedical Engineering, Duke University, Durham, NC 27708, USA
**matt.rinehart@duke.edu*

Abstract: Quantitative phase spectroscopy is presented as a novel method of measuring the wavelength-dependent refractive index of microscopic volumes. Light from a broadband source is filtered to an ~5 nm bandwidth and rapidly tuned across the visible spectrum in 1 nm increments by an acousto-optic tunable filter (AOTF). Quantitative phase images of semitransparent samples are recovered at each wavelength using off-axis interferometry and are processed to recover relative and absolute dispersion measurements. We demonstrate the utility of this approach by (i) spectrally averaging phase images to reduce coherent noise, (ii) measuring absorptive and dispersive features in microspheres, and (iii) quantifying bulk hemoglobin concentrations by absolute refractive index measurements. Considerations of using low coherence illumination and the extension of spectral techniques in quantitative phase measurements are discussed.

OCIS codes: (120.5050) Phase measurement; (180.3170) Interference microscopy; (300.0300) Spectroscopy; (110.4234) Multispectral and hyperspectral imaging; (090.6186) Spectral holography; (170.0170) Medical optics and biotechnology.

References and links

1. M. T. Rinehart, T. K. Drake, F. E. Robles, L. C. Rohan, D. Katz, and A. Wax, "Time-resolved imaging refractometry of microbicidal films using quantitative phase microscopy," J. Biomed. Opt. **16**(12), 120510 (2011).
2. Y. Park, T. Yamauchi, W. Choi, R. Dasari, and M. S. Feld, "Spectroscopic phase microscopy for quantifying hemoglobin concentrations in intact red blood cells," Opt. Lett. **34**(23), 3668–3670 (2009).
3. D. Fu, W. Choi, Y. Sung, Z. Yaqoob, R. R. Dasari, and M. Feld, "Quantitative dispersion microscopy," Biomed. Opt. Express **1**(2), 347–353 (2010).
4. M. T. Rinehart, N. T. Shaked, N. J. Jenness, R. L. Clark, and A. Wax, "Simultaneous two-wavelength transmission quantitative phase microscopy with a color camera," Opt. Lett. **35**(15), 2612–2614 (2010).
5. B. Rappaz, F. Charrière, C. Depeursinge, P. J. Magistretti, and P. Marquet, "Simultaneous cell morphometry and refractive index measurement with dual-wavelength digital holographic microscopy and dye-enhanced dispersion of perfusion medium," Opt. Lett. **33**(7), 744–746 (2008).
6. M. A. Choma, A. K. Ellerbee, S. Yazdanfar, and J. A. Izatt, "Doppler flow imaging of cytoplasmic streaming using spectral domain phase microscopy," J. Biomed. Opt. **11**(2), 024014 (2006).
7. Z. Monemhaghdoust, F. Montfort, Y. Emery, C. Depeursinge, and C. Moser, "Dual wavelength full field imaging in low coherence digital holographic microscopy," Opt. Express **19**(24), 24005–24022 (2011).
8. Z. Yaqoob, T. Yamauchi, W. Choi, D. Fu, R. R. Dasari, and M. S. Feld, "Single-shot full-field reflection phase microscopy," Opt. Express **19**(8), 7587–7595 (2011).
9. N. T. Shaked, Y. Zhu, M. T. Rinehart, and A. Wax, "Two-step-only phase-shifting interferometry with optimized detector bandwidth for microscopy of live cells," Opt. Express **17**(18), 15585–15591 (2009).
10. Life Technologies, "FluoSpheres®," http://probes.invitrogen.com/media/spectra/data/8809h2o.txt.
11. R. K. Ahrenkiel, "Modified Kramers-Kronig analysis of optical spectra," J. Opt. Soc. Am. **61**(12), 1651–1655 (1971).
12. F. E. Robles, L. L. Satterwhite, and A. Wax, "Nonlinear phase dispersion spectroscopy," Opt. Lett. **36**(23), 4665–4667 (2011).
13. P. Schiebener, J. Straub, J. M. H. Levelt Sengers, and J. S. Gallagher, "Refractive index of water and steam as function of wavelength, temperature and density," J. Phys. Chem. Ref. Data **19**(3), 677–717 (1990).
14. F. E. Robles, S. Chowdhury, and A. Wax, "Assessing hemoglobin concentration using spectroscopic optical coherence tomography for feasibility of tissue diagnostics," Biomed. Opt. Express **1**(1), 310–317 (2010).
15. O. Zhernovaya, O. Sydoruk, V. Tuchin, and A. Douplik, "The refractive index of human hemoglobin in the visible range," Phys. Med. Biol. **56**(13), 4013–4021 (2011).
16. R. Barer, "Refractometry and interferometry of living cells," J. Opt. Soc. Am. **47**(6), 545–556 (1957).

#164551 - $15.00 USD Received 14 Mar 2012; revised 5 Apr 2012; accepted 10 Apr 2012; published 12 Apr 2012

1. Introduction

Quantitative phase microscopy (QPM) has developed into an effective tool for measuring spatial and temporal properties of semitransparent samples, especially *in vitro* cells and microfluidic systems [1]. Recent interest has turned toward the wavelength dependence of refractive index in the context of QPM. Park et al. demonstrated the ability to measure pure solutions of bovine serum albumin and hemoglobin using a white light source and seven color filters with various center wavelengths [2]. They further showed that it was possible using three specific wavelengths to measure spatial distributions of hemoglobin within individual blood cells [2]. Fu et al. used a two-wavelength QPM system to measure and map dispersion in live HeLa cells [3]. Multi-wavelength illumination has also been employed to aid phase unwrapping [4] and to decouple refractive index from cell thickness [5]. All of these methods exploit dispersive effects in QPM at small numbers of discrete spectral points.

Here, we introduce quantitative phase spectroscopy (QPS) as a method of investigating spatially-resolved dispersion in microscopic samples. QPS combines microscopic quantitative phase measurements with a rapidly-tunable broadband source. In addition to producing spatially-resolved quantitative dispersion information, QPS phase images can be spectrally averaged to reduce coherent noise. We demonstrate the utility of this new technique by characterizing dispersion differences between fluorescent and non-fluorescent microspheres. We also use this instrument to measure the absolute refractive index as a function of wavelength in bulk hemoglobin solutions.

2. Theory

2.1. Quantitative phase spectroscopy (QPS)

QPM is readily extended into QPS by either sweeping the center wavelength of a narrowband source or using a tunable filter with a broadband source and acquiring interferometric data at multiple discrete wavelength steps. While swept source lasers and some tunable filters can have extremely narrow output lines, this paper focuses on the specific application of an acousto-optic tunable filter with a supercontinuum source. The resulting illumination spectra are broad enough (~5 nm) that temporal coherence effects are evident in the off-axis interferograms.

2.2. Low-coherence off-axis interferometry

Consider the intensity recorded by a digital camera from interference between monochromatic sample and reference fields: $I\left(k,\vec{r}\right)=I_S\left(k,\vec{r}\right)+I_R\left(k,\vec{r}\right)+I_{INT}(k,\vec{r})$, where $k = 2\pi/\lambda$ and $\vec{r}$ is a two-dimensional spatial vector. The first two terms are the intensities of each individual field and I_{INT} is an interferometric term containing cross correlated information about the two fields. Within the framework of off-axis interferometry with plane wave illumination, the interference term may be written as: $I_{INT} \propto Re\{e^{i(k\vec{\theta}\cdot\vec{r}+k\delta z+\Delta\varphi(k,\vec{r}))}\}$, where $\vec{\theta}$ is a vector of the Cartesian-coordinate angular difference between the sample and reference plane waves; δz is the average optical path length (OPL) difference between the two interferometer arms; and $\Delta\varphi\left(k,\vec{r}\right)$ encompasses the spatially- and wavelength-dependent phase delays, relative to the average OPL, imparted by the semitransparent sample. Extending the interference term to describe a source with a finite spectral extent, modeled here as a Gaussian distribution, yields a detected interference term that is integrated across the wavenumber spectrum:

$$I_{det}(k_0,\vec{r}) \propto \int_0^\infty e^{\frac{-(k-k_0)^2}{\delta k^2}} Re\left\{e^{i\left(k\vec{\theta}\cdot\vec{r}+k\delta z+\Delta\varphi(k,\vec{r})\right)}\right\}\,dk. \qquad (1)$$

#164551 - $15.00 USD Received 14 Mar 2012; revised 5 Apr 2012; accepted 10 Apr 2012; published 12 Apr 2012

Here, $k_0 = 2\pi / \lambda_0$ is the center wavenumber and δk is a measure of the spectral bandwidth of the illumination. If the dispersion of $\Delta\varphi$ is small relative to this spectral bandwidth, $\Delta\varphi(k,\vec{r})$ simplifies to $\Delta\varphi(k_0,\vec{r})$, in which the wavenumber is treated as constant across this integral. Integrating the remaining terms yields

$$I\left(k_0,\vec{r}\right) \propto Re\left\{ e^{i\,\Delta\varphi(k_0,\vec{r})} \cdot e^{-ik_0\left(\vec{\theta}\cdot\vec{r}+\delta z\right)} \cdot e^{\frac{-\left(\vec{\theta}\cdot\vec{r}+\delta z\right)^2 \delta k^2}{4}} \right\}. \qquad (2)$$

The first exponential term in Eq. (2) describes the relative phase delays of the semitransparent sample object at location $\vec{r}$; the second exponential term is the high-frequency spatial carrier; and the third exponential term describes the complex amplitude coherence envelope that modulates the interferometric information. It is important to note that both the angular carrier frequency and the spatial fringe visibility dictated by the coherence envelope are set by $\vec{\theta}$, and thus a fixed number of fringes are visible for a given spectral bandwidth δk. As can be seen in Figs. 1(A)–1(B) and 1(E)–1(F), an increase of δk from 1 nm to 5 nm reduces the number of fringes visible, and in Figs. 1(B)-1(C) and 1(F)-1(G), a 20 µm change in bulk path delay δz between the two interferometer arms causes the fringes to shift to a different lateral section of the field of view. The primary consequence of such a finite spectral bandwidth in the context of off-axis interferometry is that the phase sensitivity at the edges of the field of view decreases as the width of the complex envelope decreases [6]. Several groups have investigated the use of diffractive optical elements to alleviate this effect when using a large spectral bandwidth [7,8].

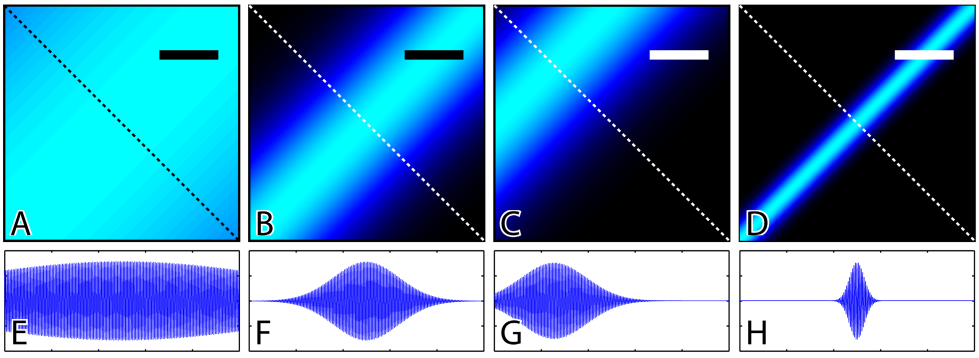

Fig. 1. Simulation of the effects of low coherence illumination on off-axis QPM carrier frequency (λ_0 = 500 nm): (A-D) Amplitude of complex envelope (term 3 of Eq. (2) of the interference cross-term. (E-H) High-frequency spatial modulation (term 2 of Eq. (2) cross-sections from dotted lines in corresponding (A-D). (A,E) δz = 0 µm, $\delta\lambda$ = 1 nm; some roll-off of amplitude is seen. (B,F) δz = 0 µm, $\delta\lambda$ = 5 nm; amplitude roll-off obscures signal at edges of field of view. (C,G) δz = 20 µm, $\delta\lambda$ = 5 nm; peak of coherence envelope moves across field of view due to path length offset. (D,H) δz = 0 µm, $\delta\lambda$ = 22 nm, ; large bandwidth severely limits field of view. Note that the angle between the sample and reference beams, and hence the spatial carrier frequency, are fixed in all of these figures. Lateral scale bars: 50 µm.

2.3. Spectral averaging of phase measurements

As illustrated in Figs. 1(D) and 1(H), traditional off-axis QPM with a large spectral bandwidth results in a narrowed field of view due to the low temporal coherence; however, this also permits high-SNR phase measurements with reduced coherent noise. On the other hand, quantitative phase images with a narrow bandwidth source benefit from a wide field of view but often suffer from coherent artifacts arising from speckle and spurious reflections. In a QPS setup using narrow-band illumination, coherent noise artifacts can be significantly improved by spectral averaging of phase measurements. In cases where the phase delay of light

#164551 - $15.00 USD Received 14 Mar 2012; revised 5 Apr 2012; accepted 10 Apr 2012; published 12 Apr 2012

transmitted through a material is linear in k (i.e., no chromatic dispersion), averaging the phase images across a range of spectral points, k_0^i, yields

$$\overline{\Delta\varphi}\left(k_0',\vec{r}\right)=\frac{\sum_{i=1}^{N}\left\{\Delta\varphi\left(k_0^i,\vec{r}\right)\right\}}{N}, \tag{3}$$

where $k_0^{'}=mean(k_0^1,k_0^2,k_0^3,\ldots,k_0^N)$. The resulting phase image $\overline{\Delta\varphi}\left(k_0^{'},\vec{r}\right)$ maintains both the wide field of view and extended axial range afforded by narrowband illumination at each k_0 while reducing the magnitude of coherent artifacts to a similar extent as would be achieved by illuminating with the full spectral bandwidth. It is important to note that when higher order k-dependencies of phase are present (e.g., material dispersion), $\overline{\Delta\varphi}\left(k_0^{'},\vec{r}\right)$ is a first-order approximation of $\Delta\varphi\left(k_0^{'},\vec{r}\right)$ and a more detailed calculation is needed to determine the average $k_0^{'}$ over the spectral illumination range.

2.4. Calculation of relative and absolute refractive index

The relative phase delays, written as $\Delta\varphi(k_0,\vec{r})$ in the first exponential term in Eq. (2), are related to the optical path length and absolute refractive index as $\Delta\varphi\left(k_0,\vec{r}\right)/k_0=\Delta n\left(k_0,\vec{r}\right)\cdot d\left(\vec{r}\right)=\Delta OPL(k_0,\vec{r})$. By rearranging this equation to solve for Δn, it becomes clear that calculating relative dispersion requires knowledge of the object thickness $d\left(\vec{r}\right)$ and that calculation of the absolute refractive index at a specific point requires a calibrated refractive index standard at another point within the field of view against which to reference the phase measurement [1]. With both of these reference quantities known, the refractive index as a function of wavelength at any point within the field of view can be calculated as

$$n_2\left(k_0,\vec{r}\right)=\frac{\Delta\varphi\left(k_0,\vec{r}\right)}{k_0 d\left(\vec{r}\right)}+n_1\left(k_0,\vec{r}\right), \tag{4}$$

where $\Delta\varphi$ is the difference in phase between points 1 and 2, n_1 is the reference point with a previously-characterized refractive index spectrum, and n_2 is the refractive index spectrum at the point of interest. It is important to note that in order to calculate the absolute refractive index, $\Delta\varphi\left(k_0,\vec{r}\right)$ must be accurately unwrapped and is limited to a range of phase delays defined by the coherence length of the source.

3. Experimental setup and methods

QPS is implemented using a modified Mach-Zehnder off-axis interferometer similar to that described previously [4]. Light from a supercontinuum laser source is spectrally filtered to a narrow band by a rapidly-tunable acousto-optic filter, coupled into a single-mode fiber, and linearly polarized before entering the interferometer. The interferometer contains adjustable path length-matching optics and compensating glass coverslips in the reference arm to offset differences in bulk dispersion arising from the sample and other interferometer optical elements. The tuning of the spectral filter is synchronized to the camera acquisition by software triggering, thus enabling an arbitrary spectral sweep and dwell pattern that is configurable based on the specific application. Off-axis interferograms acquired at each center wavenumber, k_0, are digitally processed individually to yield two-dimensional quantitative phase images; all images are referenced to a suitable background point within the field of view.

#164551 - $15.00 USD Received 14 Mar 2012; revised 5 Apr 2012; accepted 10 Apr 2012; published 12 Apr 2012

For the experiments demonstrated in this paper, the filtered output of a supercontinuum laser (SC450-2-AOTF, Fianium) was tuned from 500 to 720 nm in 1 nm steps with a FWHM bandwidth ranging from 3.8 nm at λ_0 = 460 nm to 8.2 nm at λ_0 = 720 nm. Tuning was performed by an acousto-optic tunable filter with input RF waveforms synthesized by a programmable frequency synthesizer (iDDS-2-SE, Isomet). Interferograms were acquired with a high speed CMOS camera with 20 µm square pixels (Fastcam SA4, Photron) using a 2.5 ms integration time and a 20 ms delay between tuning steps, resulting in a 5.5 s acquisition time for a sweep that comprises the majority of the visible spectrum. Imaging and wavefront matching optics consisted of 100×, 0.9 NA dry objectives with a 1mm working distance (Nikon) in 4F image relay configuration with an F = 200 mm achromatic tube lens. The angle between the reference and sample beams at the detector was set to $\theta_x,\theta_y \approx 6.25$ mrad, yielding a fringe frequency of 1 cycle/ 4px at λ_0 = 500 nm and 1 cycle/5.76 px at λ_0 = 720 nm. This range of carrier fringe frequencies was chosen to optimally use the camera's spatial frequency bandwidth for off-axis interferometry [9].

The acquired interferograms were each processed to yield quantitative phase images according to methods described in our previous work [1]. It is important to note that the fringe modulation frequency in term 2 of Eq. (2) is a function of k_0 and thus changes as the center illumination wave number is tuned. Therefore the spatial filtering step in the digital phase retrieval algorithm must be tailored for each acquired interferogram based on previous system characterization.

4. Experimental results & discussion

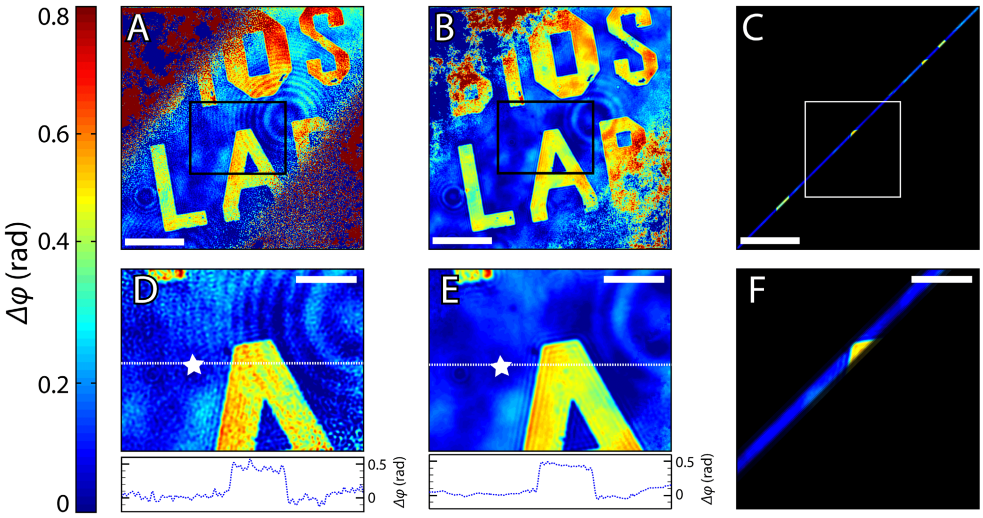

Fig. 2. Phase images of a transparent PDMS phase object, demonstrating a reduction of coherent noise by spectral averaging. Letters have a nominal 90nm thickness. (A,B) Full field of view (~200x200µm) with reduced SNR at the edges; 50µm scale bars. (D,E) zoomed in view with insets corresponding to plots at the dotted lines; 20µm scale bars. (A,D) imaged with λ_0 = 603 nm, $\delta\lambda$ = 5.4 nm; (B,E) computed by averaging 220 phase maps across 500–720 nm, λ_0' = 603 nm . (C,F) Simulation of a phase image acquired with $\delta\lambda$ = 220 nm; note the area over which high-SNR phase information is significantly reduced.

4.1. Coherent noise reduction

A custom-molded phase target was used to demonstrate coherent noise reduction across a wide field of view. The phase target was molded by casting PDMS (polydimethylsiloxane, Sylgard 184, Dow Corning) on top of a custom fabricated photomask (Photo Sciences Inc.) with 90 nm nominal thickness chrome features, consisting of the words '*BIOS LAB*', on a

#164551 - $15.00 USD Received 14 Mar 2012; revised 5 Apr 2012; accepted 10 Apr 2012; published 12 Apr 2012

glass substrate. After molding, the PDMS was peeled off of the photo mask and placed feature-side-up on a microscope coverslide. A quantitative phase image of this sample, acquired using λ_0 = 603 nm, $\delta\lambda$ = 5.4 nm is shown in Figs. 2(A) and 2(D). This image suffers from coherent noise and exhibits degraded phase information at the edges of the field of view, as predicted by Eq. (2). Figures 2(B) and 2(E) show a composite phase image of the target computed by spectrally-averaging 220 quantitative phase images acquired in 1 nm intervals across the 500–720 nm bandwidth. The effective center wavelength, computed as $\lambda' = 2\pi / k_0'$ (see Subsection 2.3), is $\lambda_0' = 603$ nm. While the field of view is comparable for both images, the coherent noise is significantly reduced in the spectrally-averaged phase image. The remaining variations in measured thickness that are still visible are primarily due to smooth changes in the molded PDMS thickness. Note that the improved SNR reveals the bottom half of the first letter "B", which is overwhelmed by phase noise in Fig. 2(A). The standard deviation of a flat background area denoted by the star symbols in Fig. 2(D) and 2(E) are σ = 27.7 mrad and σ = 8.6 mrad, respectively. This demonstrates a factor of ~3.2× reduction in the amplitude of spatially-dependent coherent noise artifacts achieved by spectral averaging.

For comparison, we consider an alternative method of reducing coherent artifacts by illuminating the sample with the entire spectral range in a single shot, corresponding to an even lower degree of coherence. However, according to Eq. (2) and as illustrated in Fig. 1, only a few fringes would be visible when using traditional off-axis QPM. The area of high-SNR phase measurements would be limited to a fraction of the total field of view. Figures 2(C) and 2(F) simulate the phase image field that would be visible if illuminated with a spectral range of 500–720 nm simultaneously.

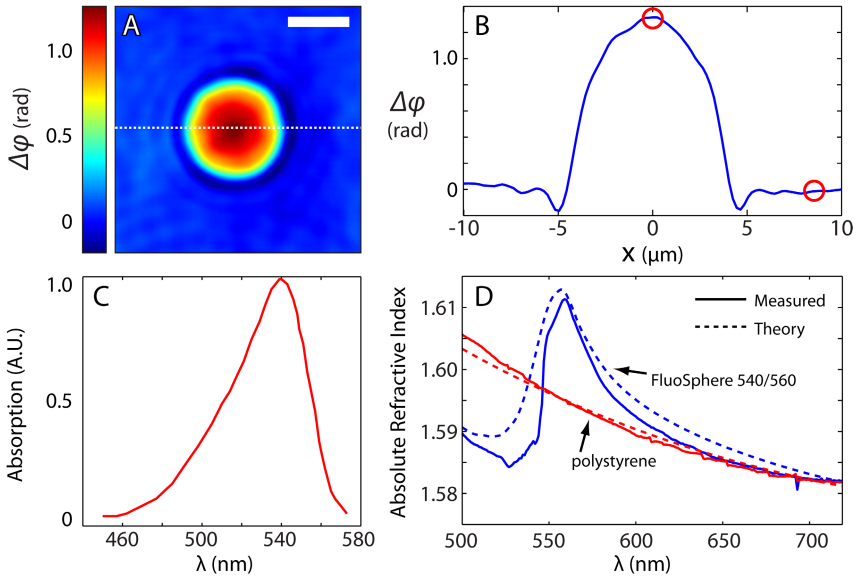

Fig. 3. (A) Phase images of a fluorescent 10μm polystyrene microsphere, λ_0' = 594 nm; scale bar is 5 μm. (B) Phase profile taken from dashed line (A). (C) Published absorption peak of fluorescent microsphere [10]. (D) Theoretical and measured absolute refractive index spectra of fluorescent and non-fluorescent microspheres, calculated from the points circled in (B).

4.2. Phase measurements of absorptive features

According to the Kramers-Kronig relation, absorption peaks in a sample give rise to nonlinear features in the real refractive index [11,12]. In this section, we examine the ability of QPS to recover spectroscopic data from phase images using fluorescent (F-8833, Life Technologies) and non-fluorescent (Duke Scientific) 10μm polystyrene microspheres as samples. The

#164551 - $15.00 USD Received 14 Mar 2012; revised 5 Apr 2012; accepted 10 Apr 2012; published 12 Apr 2012

microspheres were immersed in index-matching oil (Series A, Cargille Labs), $n_D = 1.5900$, and imaged using QPS as described above. Figure 3(A) shows the quantitative phase map of the fluorescent microsphere, $\overline{\Delta\varphi}$, calculated by averaging phase images from 500 to 700 nm, $\lambda_0' = 594$ nm. Using a background point as a reference for the relative delays through the center of the microsphere (red encircled points in Fig. 3(B)), the absolute refractive index was calculated according to Section 2.4 by adding the computed Δn to the refractive index spectrum of the immersion oil. Figure 3(C) shows the absorption peak published for the fluorescent microsphere [10]. Figure 3(D) shows the measured and theoretical refractive indices of the fluorescent (blue line) and non-fluorescent (red line) microspheres The theoretical curve for the non-fluorescent microsphere is simply the known RI of polystyrene as a function of wavelength, while the RI of the fluorescent microsphere was calculated by adding the theoretical RI of the fluorophore, as calculated by a truncated Kramers-Kronig relation [11,12], to the RI of polystyrene. The strong modulation introduced by the presence of the absorbing fluorophore is easily visible here, and shows good agreement to the theoretical predictions.

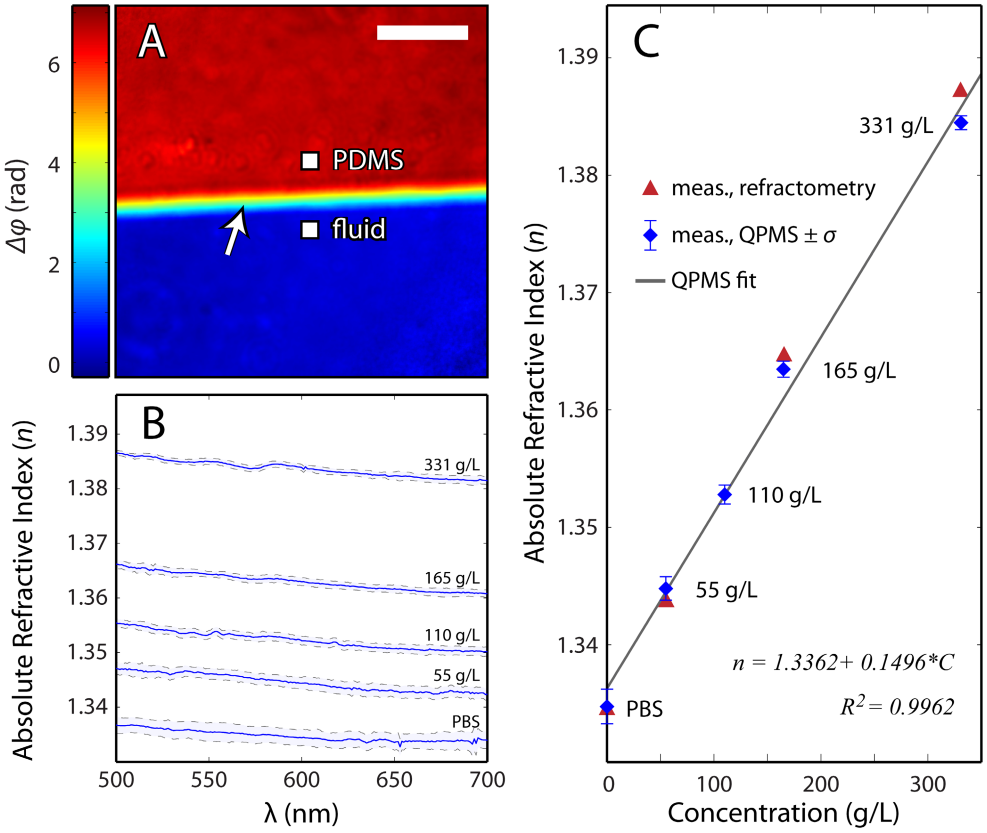

Fig. 4. (A) Phase image of PDMS chamber for bulk fluid RI spectroscopy, scale bar 25 μm. (B) Measured RI dispersion spectra for serial dilutions of oxy-hemoglobin and PBS. (C) Refractive index of measured fluids as a function of hemoglobin concentration. Blue diamonds correspond to values measured by QPS; Red triangles to values measured by a commercial refractometer. $\lambda_0 = 589$ nm; fit trend line: $n = 1.3362 + 0.1496C$, $R^2 = 0.9962$.

4.3. Hemoglobin dispersion measurements

The final proof of principle experiment presented here is the application of QPS to acquire quantitative refractive index spectra of bulk fluids. A custom-molded PDMS chamber (Fig.

#164551 - $15.00 USD Received 14 Mar 2012; revised 5 Apr 2012; accepted 10 Apr 2012; published 12 Apr 2012

4(A)) with a d = 10.5μm step height is first filled with deionized H_2O with a known refractive index [13]. Since the difference in phase, $\Delta\varphi$, between points on the top and bottom surfaces of this chamber can potentially exceed 2π, the mold was engineered to have a smooth slope of ~54.74° over the step between the PDMS area and the fluid-filled area (arrow in Fig. 4(A)) in order to enable accurate phase unwrapping [1]. The refractive index of the PDMS is treated as the sample to be measured, and is calculated using Eq. (4). The resulting spectrum is fit to a $1/k$ trend line, which is subsequently used as the reference refractive index of PDMS.

After characterizing the chamber, the water is replaced with the fluid of interest. In these experiments, we measure serial dilutions of ferrous-stabilized hemoglobin powder (H0267, Sigma-Aldrich) dissolved in phosphate buffer solution (PBS), forming oxy-hemoglobin solutions [14] with biologically-relevant concentrations of 331 g/L, 165 g/L, 110 g/L, 55 g/L, and 0 g/L (PBS). Figure 4(B) shows the refractive index spectra calculated for each of these solutions from the differential phase measurements averaged over 4 × 4μm areas, as indicated by the white squares shown in Fig. 4(A). The noise associated with this measurement, expressed by the spatial standard deviation across the points used in the measurement, is shown for each solution by the dashed gray lines. This standard deviation value monotonically decreases with increasing concentration from an average of 1.59×10^{-3} for PBS to 6.34×10^{-4} for 331 g/L oxy-hemoglobin.

To validate these measurements, the refractive index of these solutions at λ_0 = 589 nm as measured with QPS (blue diamonds in Fig. 4(C)) were compared to RI values of the same samples measured by a commercial refractometer (RFM300, Bellingham & Stanley) at λ_D = 589.3 nm (red triangles in Fig. 4(C)). These measurements show good agreement and also compare well with a recent report of direct multi-wavelength refractometry measurements of oxy-hemoglobin solutions [15]. Upon fitting the concentration-dependent measurements of refractive index data to the form originally described by Barer et al. [16]: $n = n_0 + \alpha C$, where C is in g/mL, a trend line of $n = 1.3362 + 0.1496C$ was found with an R^2 coefficient of 0.9962 and a root-mean-square-error of 1.450×10^{-3}. The concentration-dependent coefficient α closely matches the fit (α = 0.148), reported by Zhernovaya et al. [15].

5. Summary

In this paper, we have presented QPS as a novel method of investigating refractive index features with high spatial and spectral resolution. We developed a theoretical basis to model the tradeoff between coherence length and lateral field of view in off-axis holography, and described a method of spectral averaging to reduce coherent artifacts in quantitative phase images that circumvents this tradeoff. This approach was experimentally demonstrated using a transparent PDMS phantom in which we calculate an ~3.2× reduction of spatial noise to σ = 8.6 mrad when using a 220 nm spectral range, corresponding to a path length of 807 picometers. We then applied QPS to microspheres with different absorptive properties and observed distinct features in the measured RI spectra that agree with the predictions of the Kramers-Kronig relation. Finally, we measured the RI spectra of multiple oxy-hemoglobin serial dilutions using a custom-molded PDMS chamber with a fixed step height and a sloped step edge. These measurements yielded a linear dependence over a biologically-relevant concentration range that agrees with previously published direct refractometry measurements of bulk hemoglobin samples. These results both validate the method of QPS for investigating spatially-resolved RI spectra and also suggest the utility of this technique for quantifying molecular compositions based on unique absorptive and dispersive features.

Acknowledgments

We gratefully acknowledge help in the photolithography and custom PDMS molding process provided by the Duke University Shared Materials Instrumentation Facility (SMIF). This research was supported by National Science Foundation grant MRI-1039562.

#164551 - $15.00 USD Received 14 Mar 2012; revised 5 Apr 2012; accepted 10 Apr 2012; published 12 Apr 2012